International Journal of Wildland Fire 25(1) 48–61
doi: 10.1071/WF15090_AC

Supplementary material

Measuring radiant emissions from entire prescribed fires with ground, airborne, and satellite sensors – RxCADRE 2012

Matthew B. Dickinson[A,M], *Andrew T. Hudak*[B], *Thomas Zajkowski*[C,K], *E. Louise Loudermilk*[D], *Wilfrid Schroeder*[E], *Luke Ellison*[F,G], *Robert L. Kremens*[H], *William Holley*[I,L], *Otto Martinez*[I,L], *Alexander Paxton*[I], *Benjamin C. Bright*[B], *Joseph J. O'Brien*[D], *Benjamin Hornsby*[D], *Charles Ichoku*[F], *Jason Faulring*[H], *Aaron Gerace*[H], *David Peterson*[J] *and Joseph Mauceri*[H]

[A]USDA Forest Service, Northern Research Station, 359 Main Road, Delaware, OH 43015, USA.

[B]USDA Forest Service, Rocky Mountain Research Station, Forestry Sciences Laboratory, 1221 South Main Street, Moscow, ID 83843, USA.

[C]USDA Forest Service, Remote Sensing Applications Center, 2222 W. 2300 South Salt Lake City, UT 84119, USA.

[D]USDA Forest Service, Center for Forest Disturbance Science, Southern Research Center, 320 Green Street, Athens, GA 30602, USA.

[E]Department of Geographical Sciences, University of Maryland, College Park, MD 20742, USA.

[F]NASA Goddard Space Flight Center, 8800 Greenbelt Road, Greenbelt, MD 20771, USA.

[G]Science Systems and Applications, Inc., 10210 Greenbelt Road, Suite 600, Lanham, MD 20706, USA.

[H]Rochester Institute of Technology, Center for Imaging Science, 54 Lomb Memorial Drive, Rochester, NY 14623, USA.

[I]US Air Force, 96th Test Wing, Eglin Air Force Base, Niceville, FL 32542, USA.

[J]National Research Council, 7 Grace Hopper Avenue, Monterey, CA 93943, USA.

[K]Present address: Institute for Transportation Research and Education, North Carolina State University, Raleigh, NC 27695, USA.

[L]Deceased.

[M]Corresponding author. Email: mdickinson@fs.fed.us

Accessory publication 1:

Calibration procedure for single-band WASP LWIR data - incorporating spectral sensor response and atmospheric transmission

Matthew B. Dickinson[A,C] *and Robert L. Kremens*[B]

[A]USDA Forest Service, Northern Research Station, 359 Main Road, Delaware, OH 43105, USA.

[B]Rochester Institute of Technology, Center for Imaging Science, 54 Lomb Memorial Drive, Rochester, NY 14623, USA.

[C]Corresponding author: Email: mdickinson@fs.fed.us

We describe a calibration approach providing total ground-leaving radiative excitance (W m^{-2}), also termed fire radiated flux density (FRFD), from the response of a limited-bandpass infrared sensor. The resulting calibration relationships are specific to individual fires because spectral atmospheric transmission data are incorporated. Here we report calibration relationships for the RxCADRE 2011 and 2012 WASP data collections. Calibration of the WASP longwave infrared (LWIR) sensor (8 to 9.2 μm nominal bandpass) (Fig. AP1-1) involves relating total ground-leaving radiance (W m^{-2} sr^{-1}) from 0.1 to 20 μm (accounting for almost all fire radiation) to WASP raw output (digital number, DN) through a number of linked steps. The general calibration equation is

$$L_T = bL_{LWIR}{}^{M} \quad (1)$$

where L_T (W m^{-2} sr^{-1}) is total ground-leaving radiance; L_{LWIR} is detector-reaching radiance in the passband of the WASP LWIR detector during flights over wildland fires; and *b* and *M* are parameters relating restricted-bandpass to total radiance. The inclusion of a unit solid angle in steradians for dimensional consistency is implied (see Palmer and Grant 2009, eq. 2.32). The WASP Indigo Phoenix LWIR camera (model IA126 LWIR) was built by Cantronic Systems Incorporated and has quantum-well, cooled detectors. The WASP LWIR camera has 14 bits of dynamic range and is cooled by a Stirling cooler to about 60°K.

The first step in the calibration process is to relate DN to calculated blackbody radiance in the bandpass of the sensor. For calibration measurements, the blackbody and WASP sensor were placed well off the floor and surrounding areas wrapped in foil to avoid background effects on calibration measurements. The distance between the blackbody and sensor was set so that the blackbody filled more than 40 central pixels. In this near extended–source configuration (NES) (Palmer and Grant 2009, section 7.6.4), the blackbody is close enough to the sensor so that pixels are much smaller than the heated area and radiance reaching the front of the lens is equal to blackbody radiance. The average of pixel DN for a given blackbody temperature is calculated for only the central region of the blackbody where temperatures are uniform. A swing-in blackbody calibrator that is now used during WASP operation and shows that there is minimal drift in DN associated with camera lens temperature variation during flights. The image of the blackbody was flat-fielded to account for known variation in sensor response across the field of view. A 2-ms integration time was used in WASP flight operations in order to

avoid saturation yet provide as much background radiance information as possible during fire imaging missions.

Radiance leaving the blackbody and causing a response by the detector (detector-reaching radiance, L_{LWIR}) is a function of blackbody temperature and emissivity along with properties of the sensor. L_{LWIR} is determined over a range of blackbody temperatures (280–1601°K) through integration of Planck's radiation law,

$$L_{LWIR} = \varepsilon t_L \int_0^{\lambda_{max}} f(T, L_\lambda, R_\lambda) \quad (2)$$

where the integral is evaluated from 0 μm to λ_{max} (20 μm), ε is blackbody emissivity (0.95), t_L is proportional transmission of infrared radiation through the lens (0.98), T is blackbody temperature (K), L_λ is spectral radiance (W m^{-2} μm^{-1} sr^{-1}), and R_λ is proportional sensor spectral response (Fig. AP1-1). L_{LWIR} is then related to DN, which is a second-order polynomial in the case of the WASP longwave infrared sensor (Fig. AP1-2):

$$L_{LWIR} = f(DN) = 2x10^{-6}DN^2 + 0.0176DN \quad (3)$$

The parameters b and M relating L_T to L_{LWIR} in Eqn 1 are estimated from the output of 10,000 simulations of total radiative excitance from mixed-temperature fire pixels (Kremens and Dickinson 2014) (Fig. AP1-3). Estimates of total and restricted bandpass (i.e., LWIR) excitance were based on randomly generated assemblages of 30 sub-pixel areas representing the pre-frontal fuel bed, the flaming front, and the zone of post-frontal combustion and cooling. Different sub-pixel areas are defined by their temperatures and emissivities. Total excitance from these sub-pixel areas was calculated from the Stefan-Boltzmann Law and summed to give L_T. L_{LWIR} is calculated as in Eqn 2, but with the

additional effect of atmospheric absorption so that it represents WASP LWIR detector-reaching radiance during overflights:

$$L_{LWIR} = \varepsilon t_L \int_0^{\lambda_{max}} f(T, L_\lambda, R_\lambda, A_\lambda) \quad (4)$$

where A_λ is atmospheric spectral transmission calculated from MODTRAN (Table AP1-1, Fig. AP1-4).

Combining Equations 1 and 3 and converting to excitance (W m^{-2}) by multiplication of both sides of the question by π, the form of the final calibration equation for ground-leaving excitance is:

$$P_T = \pi b\big(f(DN)\big)^M \quad (5)$$

where *b* and *M* are given in Table 1 for individual fires.

References

Kremens RL, Dickinson MB (2014) Estimating radiated flux density from wildland fires from the raw output of restricted-bandpass detectors. *International Journal of Wildland Fire*, in review.

Palmer JM, Grant BG (2010) 'The art of radiometry.' (SPIE Press: Bellingham, WA). doi:10.1117/3.798237

Table AP1-1. Average atmospheric absorption estimated from MODTRAN for the large 2011 and 2012 burns

Atmospheric profile data used in MODTRAN are from soundings collected from balloons launched before ignition. Relative humidity is averaged from the surface to 3000 m. Flight altitude used was representative of the VIIRS and MODIS overpass times. Parameters *b* and *M* from Eqn 1 are estimated from a power-law fit to untransformed data because this approach, in contrast to linear regression on log-log transformed data, resulted in the least bias in background fire radiative flux density (FRFD)

Fire	Date	Launch time (UTC)	Air temperature (°K)	Relative humidity (%)	Ignition time (UTC)		Flight altitude (m)	Average transmission (8-9.2 μm)	b	M
					Start	End				
703C	06 February 2011	15:00	280	28	18:24	19:02	3030	0.88	5.216	1.374
608A	08 February 2011	14:50	285	37	18:25	19:55	2250	0.90	5.138	1.374
L1G	04 November 2012	20:31	300	48	18:30	19:46	3155	0.71	7.282	1.393
L2G	10 November 2012	20:10	296	47	18:03	21:00	3160	0.75	7.006	1.380
L2F	11 November 2012	21:49	297	50	18:23	19:05	1550	0.76	6.718	1.385

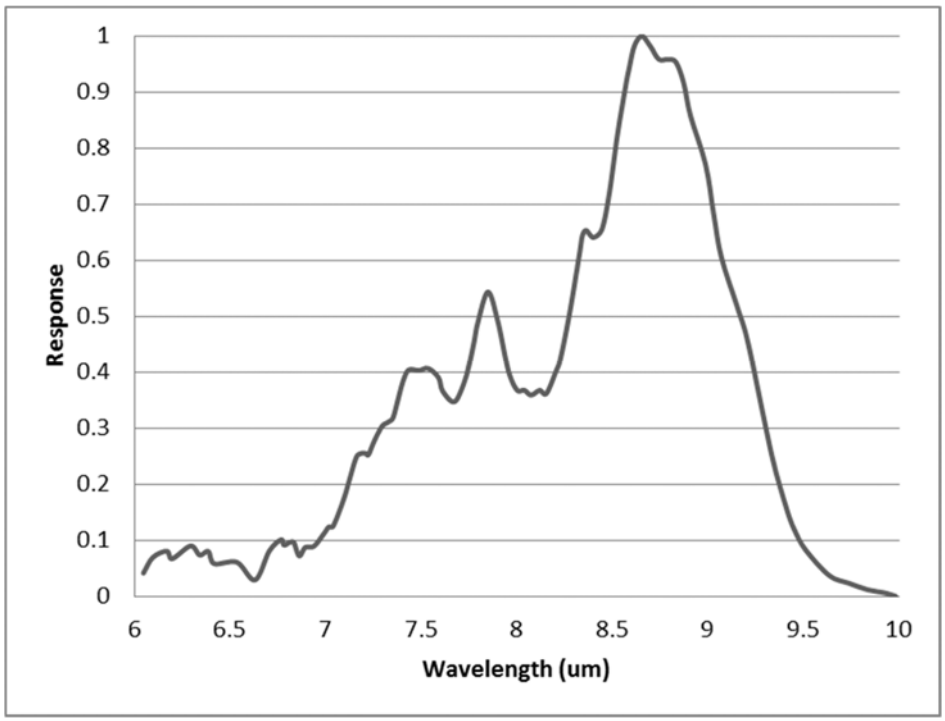

Fig. AP1-1. Spectral response of the WASP longwave infrared sensor. The nominal bandpass of the sensor is 8–9.2 μm, approximately the full width of the spectral response at 50% response (full width at one-half maximum) (FWHM).

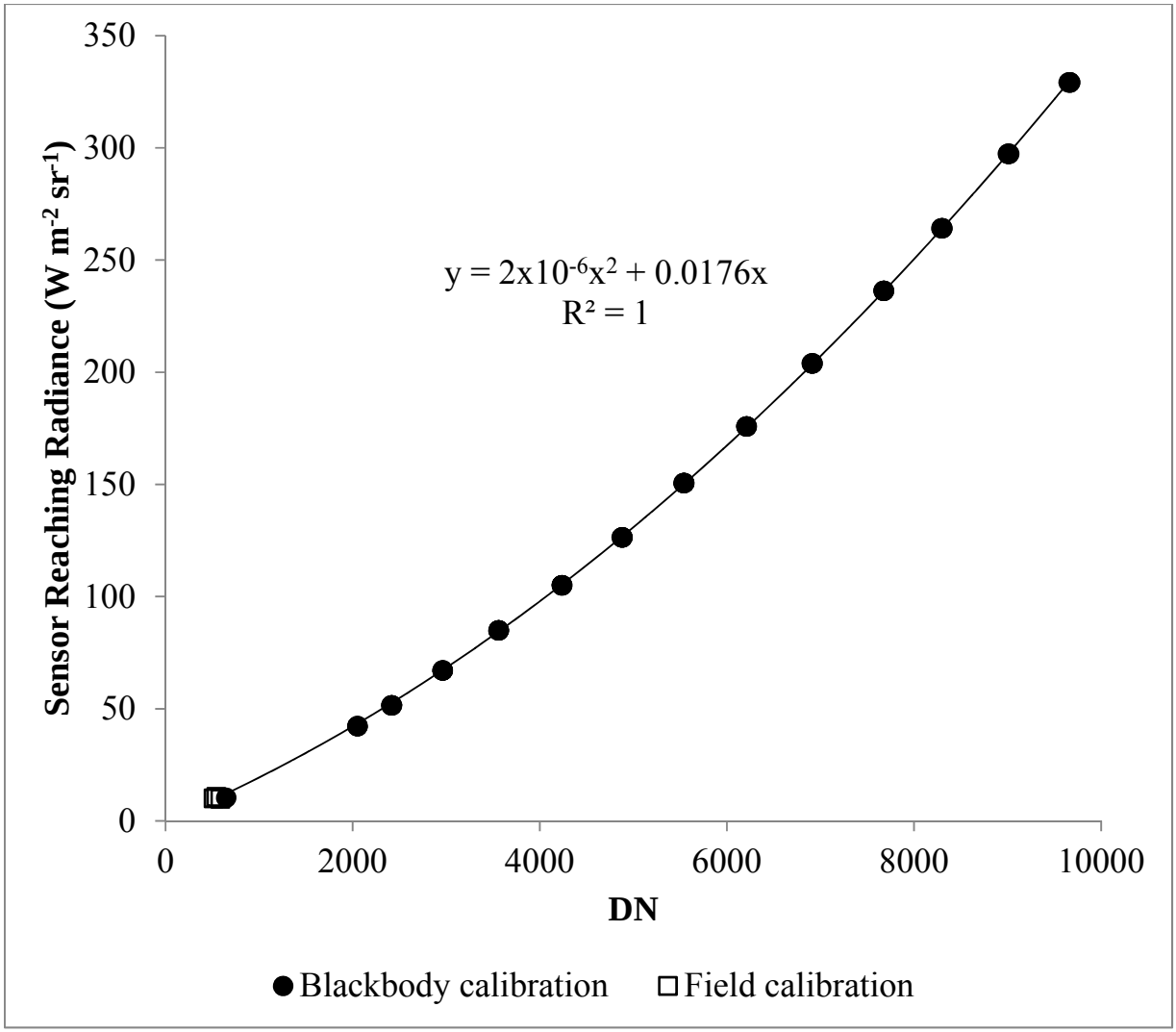

Fig. AP1-2. Calibration relationship for radiance in the WASP longwave infrared passband determined from laboratory blackbody calibration (closed circles) and three field measurements (open circles). Field measurements are average WASP background DN during three fires and detector-reaching radiance estimated for the WASP passband at the observed air temperature (see above). The polynomial regression fit only included blackbody data.

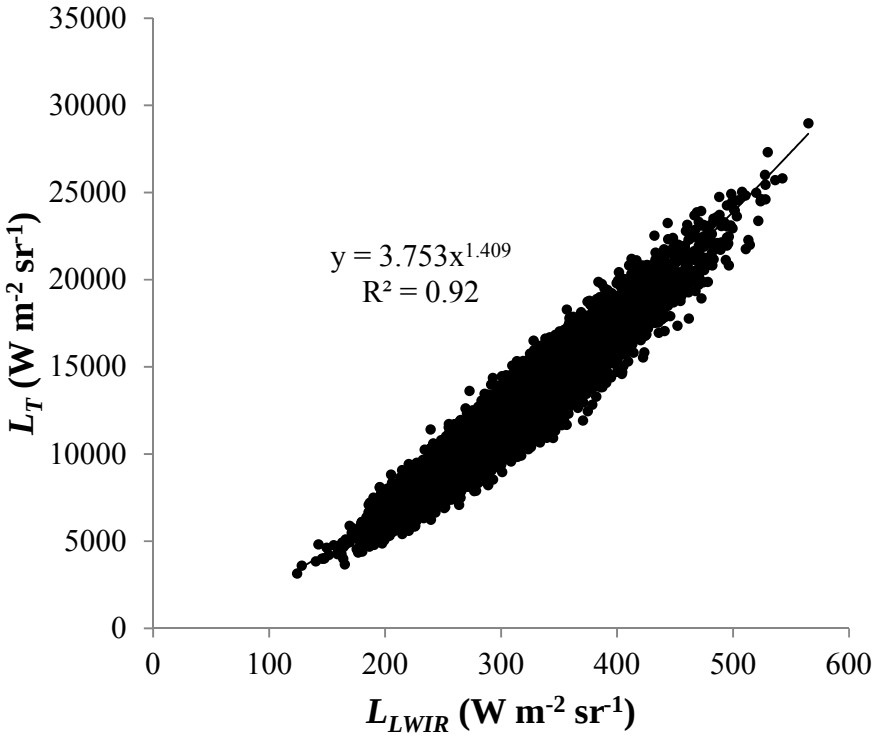

Fig. AP1-3. Power-law relationship between untransformed (total) ground-leaving and detector-reaching radiance for L2F from 10,000 fire pixel simulations. Results for other fires were similar (Table 1).

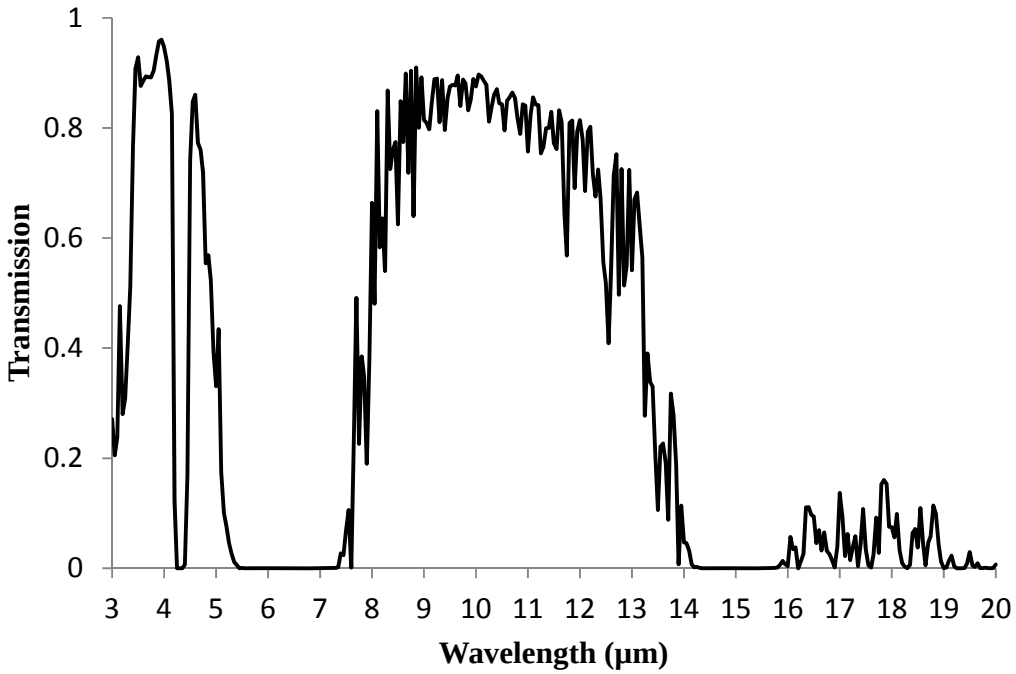

Fig. AP1-4. MODTRAN spectral atmospheric transmission for L2F based on an atmospheric profile from a mid-morning sounding conducted prior to ignition (see Table AP1-1).

Accessory publication 2:

Alternative methods for estimating fire radiated power from MODIS observations when fire boundaries are known

Luke Ellison[A,B,C] and *Charles Ichoku*[A]

[A]NASA Goddard Space Flight Center, 8800 Greenbelt Road, Greenbelt, MD 20771, USA.

[B]Science Systems and Applications, Inc., 10210 Greenbelt Road, Suite 600, Lanham, MD 20706, USA.

[C]Corresponding author: Email: luke.ellison@ssaihq.com

MODIS fire detections were obtained from the MYD14 active fire product (e.g., Giglio et al. 2003) and, of the four coincident MODIS overpass events for RxCADRE 2012 burns (S6, L1G, L2G and L2F), only two (L2G and L2F) were represented in MYD14. MODIS detected two fire pixels for the L2G burn with fire radiated power (FRP) totaling 130.9 MW, and three fire pixels from one complete scan for the L2F burn totaling 151.9 MW (see Table AP2-1, row 1). The S6 burn signal was too small to be detected in the significantly-off-nadir MODIS pixels as can be seen in Fig. AP2-1. Although the MYD14 algorithm detected an elevated signal for the L1G burn, it classified it as cloud due to the significant cloud cover over or near the fire (see Fig. AP2-1). However, in spite of the extensive cloud cover, knowing that the detected signal was indeed from the L1G fire provided the rationale to utilize the available data to retrieve FRP. This was done and a cumulative total FRP of 110.8 MW was found over four pixels for the L1G burn (Table AP2-1, row 1). The extent of attenuation of FRP by cloud cover is unknown.

In an effort to get the most realistic estimates of FRP possible, different methodologies for calculating FRP from the MODIS data were implemented for the fires. For each burn, FRP was calculated in two modes: by summation of the individually retrieved fire detections, and by clustering together all of the MODIS pixels touching the burn blocks prior to FRP retrieval (Table AP2-1, column 'Mode'). In addition to using the MYD14 default background characterizations, the small number of burns in this experiment allowed us the flexibility to manually inspect the background pixels of the MODIS fire detections. This was done to ensure that any non-clear background pixels were properly excluded from the analysis (Table AP2-1, column 'Background'). The fact that the differences between rows 1 and 3 and between 2 and 4 in Table AP2-1 are relatively small corroborates the clustering methodology. These small differences are due to the different order of calculations and the slightly different selection of background pixels. Thus, for L1G that has a high level of cloud contamination in the background, the difference between the pixel and cluster modes using the default background characterization is greater than the others. Having corroborated the clustering technique, more complete FRP values could be obtained by clustering all the pixels containing any portion of the burn plot on the ground (Table AP2-1, column 'Cluster Size').

The official MYD14 product corresponds to the first row of Table AP2-1, although the value for L1G was not available in the product but was calculated in this study based on the MYD14 algorithm. When a manual inspection of the background was done to ensure that none of the selected background pixels were contaminated (by clouds, water, smoke, significant shadows, etc.), the FRP values for L2G and L2F remained in close agreement with the MYD14 product (Table AP2-1, row 2). However, the stricter manual implementation of cloud detections yields a noticeable decrease in FRP for L1G to 94.4 MW. This value is an underestimate of L1G FRP

because, although the background was properly classified, the fire pixels still contain many clouds that lower the fire signal. Because we have confidence in the clustering method (see above), we used this method to calculate FRP for all pixels that overlap the burn blocks (see Fig. AP2-1). The clustering method yields values shown in Table AP2-1, rows 5 and 6, that are significantly higher than the corresponding prior estimates. Note that the cluster analysis was not successful for L1G in this case due to the great variability in brightness temperatures of pixels covering the fire because of the extensive cloud cover in that area. Therefore, the inclusion of non-detected parts of a fire can mitigate satellite underestimation of the whole-fire FRP output. We have the greatest confidence in the FRP estimates that are derived from the cluster method and that manually select background pixels. These FRP estimates are 151.4 MW for L2G and 174.6 MW for L2F. Due to the increased uncertainty in the L1G case from cloud attenuation of the fire signal that prevented FRP estimation using the whole-fire clustering technique, we can state with confidence only that FRP from L1G was greater than 94.9 MW.

References

Giglio L, Descloitres J, Justice CO, Kaufman YJ (2003) An enhanced contextual fire detection algorithm for MODIS. *Remote Sensing of Environment* **87**, 273–282. doi:10.1016/S0034-4257(03)00184-6

Table AP2-1. FRP values generated using different methodologies from MODIS data for the L1G, L2G and L2F burns

Each method can be described by its FRP-retrieval 'mode', background characterization, and by cluster size (if applicable). Under the 'Mode' column, 'pixels' denote hot spot determination of individual pixels followed by aggregation of their FRP values, whereas 'cluster' denotes pixel aggregation covering the fire followed by a single FRP retrieval for the whole cluster. Under the 'Background' column, 'default' denotes when the default MYD14 characterizations are used to select the background, and 'manual' denotes when the background pixels are manually selected. Under the 'Cluster Size' column, 'default' refers to the use of only pixels flagged as fire in the 'pixels' Mode, and 'all' refers to the use of all pixels that include any portion of the burn block on the ground (see Fig. AP2-1)

Methods of generating FRP			Fire radiated power		
Mode	Background	Cluster size	Burn unit		
			L1G	L2G (MW)	L2F
Pixels	Default	–	110.8	130.9	151.9
Pixels	Manual	–	94.4	130.1	155.6
Cluster	Default	Default	123.8	134.7	160.8
Cluster	Manual	Default	94.9	133.7	158.5
Cluster	Default	All	149.6	152.6	179.1
Cluster	Manual	All	–	151.4	174.6

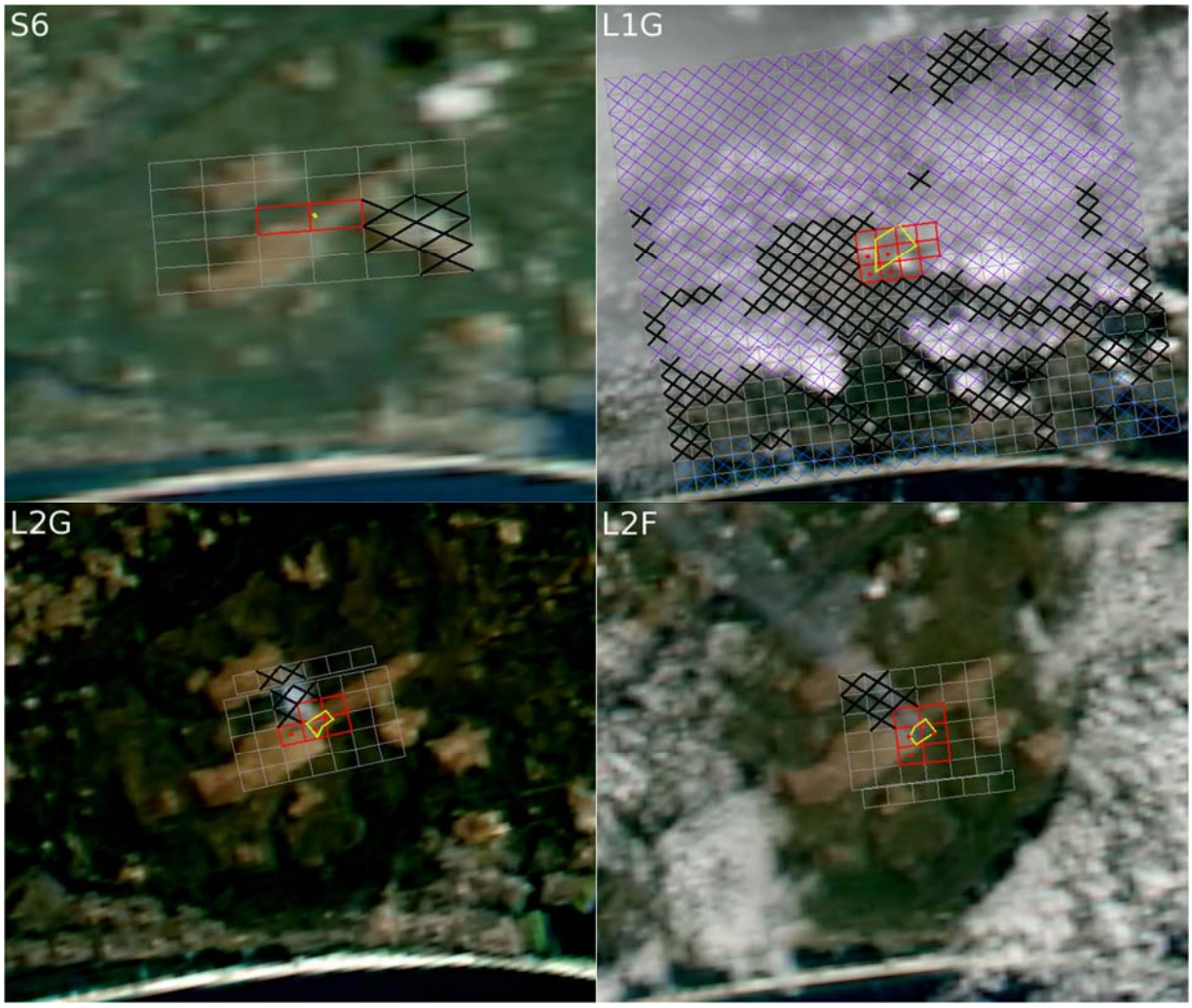

Fig. AP2-1. Diagrams of the MODIS 1-km pixels superimposed on MODIS 250-m imagery for units S6, L1G, L2G and L2F. The burn blocks are outlined in yellow, and the MODIS pixels that cover all or a portion of the burn block, keeping in mind the MODIS triangular response function that reaches halfway into the neighboring pixels along-scan, are outlined in red (Table AP2-1, rows 5 and 6). Individual pixels whose signals were strong enough to be deemed as fire detections are shown with a red dot (Table AP2-1, rows 1 and 2). Pixels excluded from the background characterization are 'X'ed out: clouds are shown in purple, water is shown in blue, and user-selected contaminated pixels are shown in thick black.